Process Safety and Environmental Protection 206 (2026) 108319

Contents lists available at ScienceDirect

Process Safety and Environmental Protection

journal homepage: www.journals.elsevier.com/process-safety-and-environmental-protection

Modelling the behaviour of cryogenic liquid hydrogen tanks engulfed in fire

Alice Schiaroli [a,b], Davide Camplese [a], Giordano Emrys Scarponi [a], Robert Eberwein [c], Federico Ustolin [b], Valerio Cozzani [a,*]

[a] LISES – Laboratory of Industrial Safety and Environmental Sustainability – Department of Civil, Chemical, Materials and Environmental Engineering, University of Bologna, via Terracini 28, Bologna 40131, Italy
[b] Norwegian University of Science and Technology (NTNU) - Department of Mechanical and Industrial Engineering, Trondheim 7491, Norway
[c] Bundesanstalt für Materialforschung und –Prüfung, Unter den Eichen 87, Berlin 12205, Germany

ARTICLE INFO

Keywords:
Liquid hydrogen
Cryogenic tanks
Fire engulfment
Multi-layer insulation
CFD modelling

ABSTRACT

The safe use of liquid hydrogen as a clean fuel requires a deep understanding of its behaviour in accident scenarios. Among other scenarios, the possible involvement of cryogenic liquid hydrogen tanks in engulfing fires is of particular concern, due to the potentially severe consequences. This study proposes a computational fluid dynamic model suitable to simulate the behaviour of liquid hydrogen tanks equipped with multi-layer insulation (MLI) engulfed in fire. An original approach has been developed to assess the progressive degradation of the performance of the thermal insulation, that is crucial in determining the tank pressurization and failure. The model is validated against full-scale experimental fire tests. The outcomes of the model reproduce the progressive pressurization and the opening time of the pressure relief valve within 2 % error. The results demonstrate the importance of accounting for the dynamic evolution of the progressive degradation of the insulation when evaluating tank pressurization, and they highlight the limitations of empirical, simplified state-of-the-art approaches. Furthermore, the analysis evidences the key role of the fire temperature in governing tank response, stressing the need for proper fire characterization to support reliable modelling of fire scenarios and the development of emergency planning and mitigation strategies ensuring the structural integrity of liquid hydrogen tanks during fire attacks.

1. Introduction

In the transition toward carbon-neutral energy systems, liquid hydrogen (LH_2) is gaining attention as a clean and efficient energy carrier, especially for high-demand sectors where energy storage density and weight constraints are critical. Cryogenic storage in double-walled tanks equipped with multi-layer insulation (MLI) offers key advantages in terms of volumetric energy density and thermal performance, in particular for bulk LH_2 transportation (Klell, 2010; Tzimas et al., 2003). However, the cryogenic conditions required for LH_2 storage, together with the high flammability of hydrogen, introduce significant safety challenges, especially in the case of accidental fire exposure, which is among the most critical threats for LH_2 storage and transportation systems. In such event, the rapid pressurization may lead to tank rupture, loss of containment, and hazardous consequences such as jet fires or boiling liquid expanding vapor explosions (BLEVEs) (Feynman, 1986; HydrogenTools Liquid, 2017; Mires, 1985). Therefore, it is crucial to have robust predictive models that can simulate the response of LH_2 tanks to external fires, both to support emergency management and to guide the development of safety measures aimed at preserving tank integrity.

Several models are available and widely used in the current practice to simulate the fire exposure of pressurized storage tanks containing liquefied hydrocarbons such as Liquefied Petroleum Gas (LPG). Most of such models are based on numerical approaches (e.g., the models from Graves, 1973; Hunt and Ramskill, 1985; Ramskill, 1988; Yu et al., 1992; Gong et al., 2004) which, due to their low computational cost and suitability for risk assessments, are preferred in industrial applications. Such models, while capable of estimating pressure rise and valve opening times, rely to different extents on adjustable parameters and simplifying assumptions, often disregarding key phenomena such as thermal stratification (Scarponi et al., 2018).

More recently, models based on computational fluid dynamics (CFD) have been introduced to overcome these limitations (e.g., see

* Corresponding author.
E-mail address: valerio.cozzani@unibo.it (V. Cozzani).

https://doi.org/10.1016/j.psep.2025.108319
Received 25 October 2025; Received in revised form 1 December 2025; Accepted 14 December 2025
Available online 15 December 2025

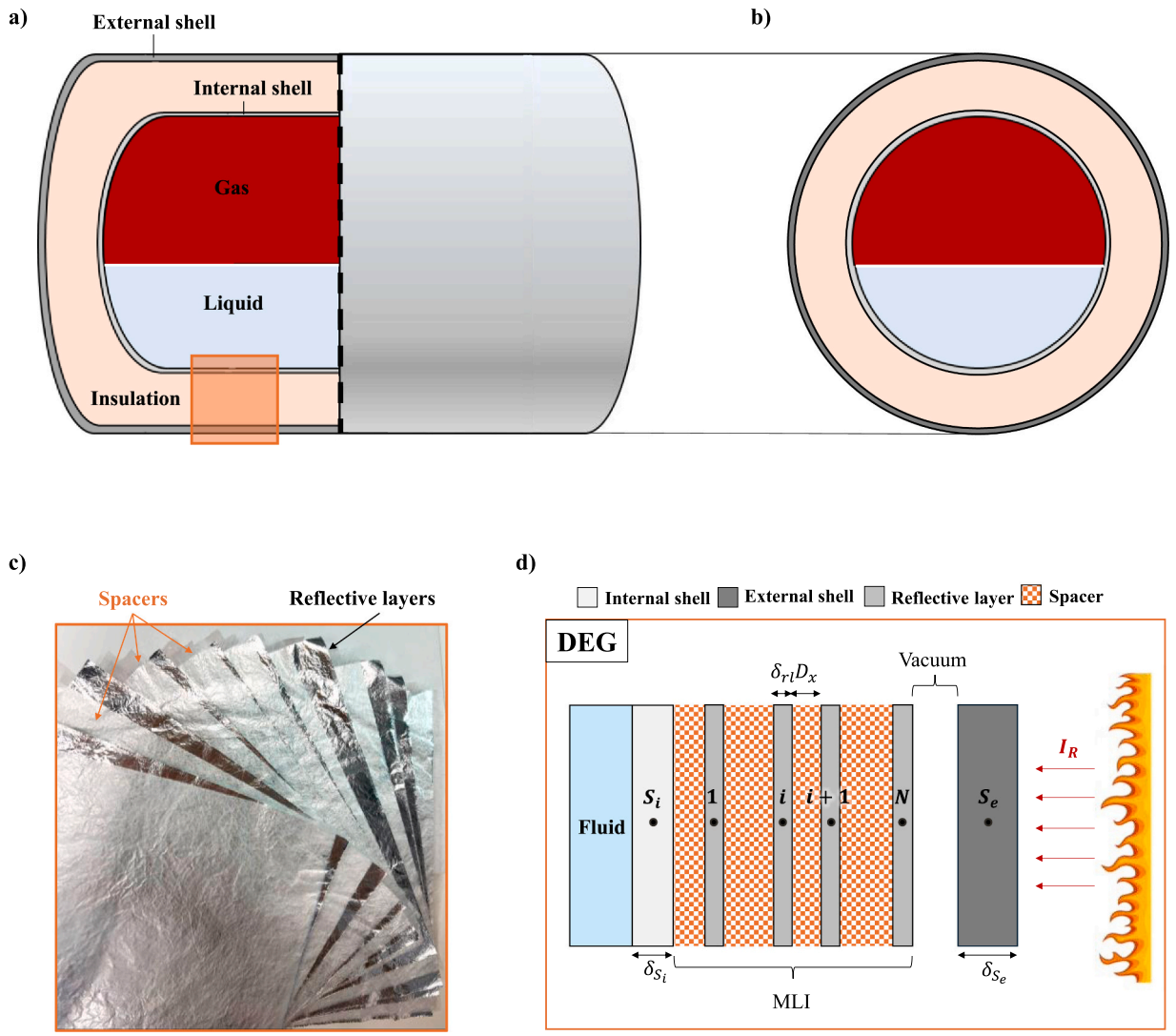

Fig. 1. a) Lateral view and b) cross-sectional view of an horizontal double-walled insulated storage tank for the storage of cryogenic liquid hydrogen; c) Structure of a multi-layer insulation with reflective layers and spacers; d) Schematization of the annular insulation space according to the MLI degradation model (see Section 2.5); MLI: Multi-layer insulation.

Hadjisophocleous et al.,1990a; Scarponi et al., 2021), although the high computational cost represents a severe limit to their adoption by industry (Scarponi et al., 2021). Most of these approaches are validated for uninsulated systems, mainly LPG tanks, while only a few are applicable to insulated storage tanks and cryogenic components. As an example, the model proposed by D'Aulisa et al. (2014a) is able to reproduce the behaviour of insulated spherical tanks containing hydrogen, propane, or methane under fire exposure. Nevertheless, its predictive capability is restricted to systems containing pressurized liquefied gases (D'Aulisa et al., 2014b). In addition, the insulation adopted in the study consisted solely of a coating layer, which is not representative of the actual cryogenic insulation systems for cryogenic liquefied hydrogen tanks. A further model, proposed by Iannaccone et al. (2021), has been validated for cryogenic Liquefied Natural Gas (LNG) tanks and may be applied to simulate multiphase cryogenic insulated vessels. However, the model only considers inorganic perlite insulation and is thus hardly applicable to vessels insulated with MLI, as those used for hydrogen transportation or fuel storage and supply onboard vehicles.

To date, only few models have been developed for the specific simulation of LH_2 tanks behaviour under engulfing fire conditions. Actually, when compared to tanks for liquefied gases at ambient temperatures and to other types of cryogenic tanks, cryogenic LH_2 vessels present additional modelling challenges. The most critical is that insulation systems can undergo rapid thermal degradation or vacuum loss during fire exposure. For instance, fire tests conducted by TNO demonstrated that the failure of the outer shell of a perlite-insulated tank can result in vacuum loss and insulation collapse, leading to rapid internal pressurization (Hulsbosch-Dam et al., 2017). In the case of MLI systems, degradation can result from melting of reflective layers or from the thermal decomposition of polymeric materials, as highlighted in recent experimental studies (Eberwein et al., 2024a).

Until now, only a lumped model (Ustolin et al., 2021) and a CFD model (Ustolin et al., 2022) were proposed for cryogenic liquid hydrogen tanks. The models were validated using experimental data from fire tests on a LH_2 tank (Pehr, 1996a). Though important and novel, these models include some important limitations. First, their validation is limited to a relatively low range of internal pressures (from atmospheric pressure up to 5 bar), below the critical point of hydrogen (National Institute of Standards and Technology, 2021). Second, important simplifications were introduced in the simulation of the behaviour of the insulation under high heat flows. Actually, the models include an empirical tuning of the values of the effective thermal conductivity of the insulation, which may not reflect the actual performance experienced during fire exposure with heat flows or fire curves different

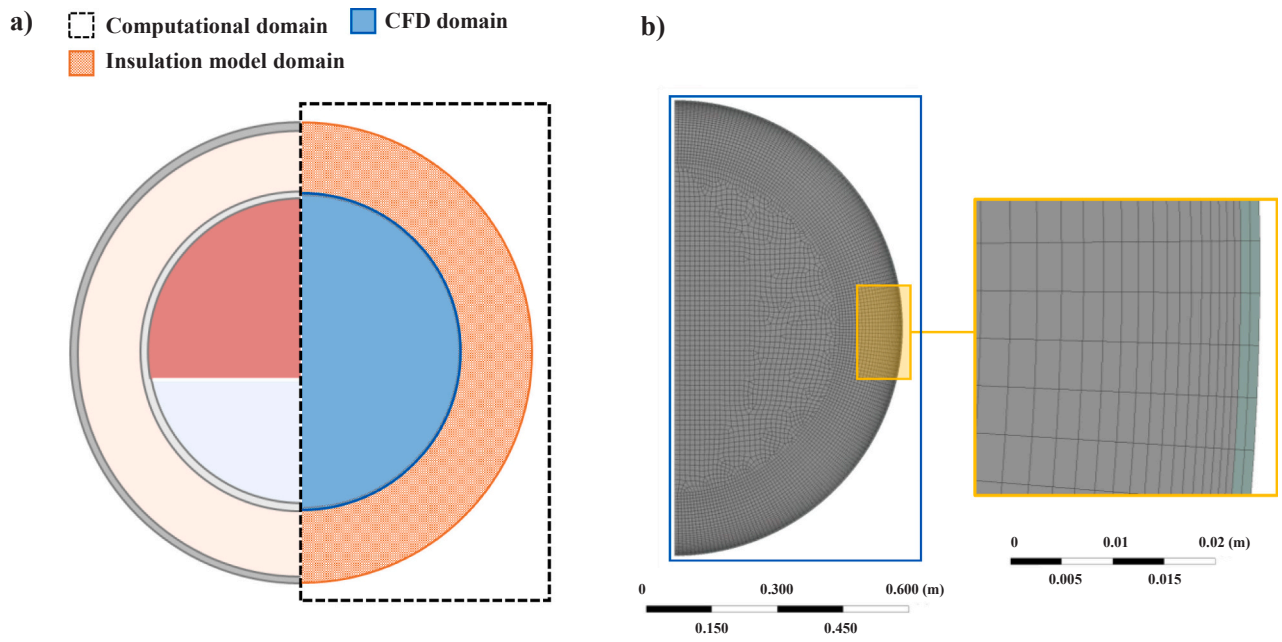

Fig. 2. a) Cross-section of the double-walled liquid hydrogen storage tank divided in the two sub-domains considered for the simulations; b) Mesh of the "CFD domain" with a zoom on the inflation layers close to the inner surface of the inner tank wall.

from those assumed in model development. Thus, depending on boundary conditions, significant uncertainties may be present when using such models, limiting the predictive accuracy of the results obtained.

Therefore, to date, a reliable and accurate model to predict the response of cryogenic LH_2 tanks under fire exposure – based on the explicit modelling of insulation performance degradation and extended to the entire pressurization range that can be expected in fire scenarios – is still missing. This study aims to fill this gap, proposing a two-dimensional (2D) CFD model designed to simulate the response of a cylindrical LH_2 tank equipped with MLI vacuum insulation when engulfed in fire. Even if a 2D approach is not able to reproduce the detail of the internal three-dimensional fluid motion and localized effects, this approach has been widely used in previous studies and proved adequate for the safety assessments of medium-size cryogenic storage tanks exposed to steady, fully engulfing fires. The 2D was thus selected since it was shown in several previous studies to represent a reasonable compromise between modelling accuracy and computational requirements, capturing the dominant heat-transfer mechanisms and providing conservative estimates of tank response in full engulfment conditions (Aydemir et al., 1988; Beynon et al., 1988; Birk et al., 2013; Chen and Lin, 1999; Gong et al., 2004; Graves, 1973b; Hadjisophocleous et al., 1990b; Hulsbosch-Dam et al., 2017; Hunt and Ramskill, 1985; Shebeko et al., 2000; Sumathipala et al., 1992).

A dynamic layer-by-layer degradation model is used to realistically characterize the insulation behaviour and degradation under high thermal loads. By integrating a CFD framework with a MLI degradation model, this study introduces an innovative and robust approach for the safety assessment of LH_2 storage systems. The model is validated against a full-scale experimental fire test, and its predictive capability is benchmarked against the state-of-the-art approaches reported in the literature.

The paper is organized as follows. In Section 2, the details of the proposed model are illustrated. In Section 3, the experimental test used for the model validation is described together with the state-of-the-art approach used to benchmark the proposed model. The results are illustrated in Section 4 and discussed in Section 5. Conclusions are drawn in Section 6.

2. Methodology

The 2D model was developed using the commercial CFD code ANSYS Fluent 18.2 (ANSYS Inc, 2018). The model features are reported in detail in the following paragraphs.

2.1. Model description

The model can simulate the behaviour of horizontal double-walled cryogenic tanks insulated with MLI and used for the storage of liquid hydrogen onboard hydrogen-powered road vehicles (e.g., passenger cars, trucks). Therefore, its applicability covers tank volumes ranging from 0.1 m^3, typical of passenger vehicles (Pehr, 1996b), up to about 1 m^3, as in the case of heavy-duty trucks or buses (Ahluwalia et al., 2023). Nevertheless, the modelling approach is also valid for larger tanks sharing the same geometry and orientation, even if for such systems the assumption of full engulfment conditions (Birk et al., 2013; Cocchi, 2022; Planas et al., 2015) and the use of MLI insulation become hardly realistic (Kang et al., 2024), thus requiring appropriate modifications. This aspect is further discussed in Section 5.

The geometry of a generic horizontal double-walled cryogenic tank is schematized in Fig. 1a (lateral section) and Fig. 1b (cross-section). The MLI insulation, consisting of multiple alternating reflective (i.e., low-emissivity) layers and high-free volume spacers arranged in a highly compact structure, is shown in Fig. 1c. The reflective layers, typically made of thin reflective plastic foils coated with metals, are designed to minimize the reflective heat transfer to the cryogenic fluid; the spacers, usually made of porous and lightweight materials, serve to maintain separation between the layers, reducing heat conduction. Finally, high vacuum is applied to minimize heat convection.

2.2. Computational domain

Exploiting the vertical symmetry of the geometry, the computational domain is defined as half of the tank cross-section, as shown in Fig. 2a (area inside the black dotted line). The overall computational domain is divided into two sub-domains, namely the "CFD domain" and the "Insulation model domain" (Fig. 2a). In ANSYS Fluent, only the "CFD domain", including the fluid zone and the inner shell, is simulated. This

Table 1
Model governing equations.

Domain	Variable	Equation Number	Equation	Nomenclature
Fluid	Momentum	Eq. (1)	$\frac{\partial(\rho\vec{u})}{\partial t}+\nabla\cdot(\rho u\vec{u}) = -\nabla p+\rho g+\nabla\cdot\left[\mu\left(\nabla\vec{u}+(\nabla\vec{u})^{T}-\frac{2}{3}\nabla\cdot u\vec{I}\right)\right]+\nabla\cdot\tau'$	$\boldsymbol{g}$: gravity acceleration $\boldsymbol{\mu}$: two-phase averaged viscosity $\boldsymbol{I}$: identity tensor
Fluid	Reynold stress tensor (with Boussinesq)	Eq. (2)	$\tau' = -\mu_T\left[\left(\nabla\vec{u}+\nabla\vec{u}^{T}\right)\right]+\frac{2}{3}(\rho K+\mu_T\nabla\cdot\vec{u}I)$	$\boldsymbol{K}$: turbulent kinetic energy
Fluid	Energy	Eq. (3)	$\frac{\partial(\rho E)}{\partial t}+\nabla\cdot[\vec{u}\quad(\rho E+p)] = \nabla\cdot\left(k_{eff}\nabla T\right)+\lambda(\dot{m}_{V\to L}-\dot{m}_{L\to V})$	$\boldsymbol{t}$: time $\boldsymbol{\rho}$: two-phase volume fraction averaged density $\boldsymbol{E}$: two-phase ensembled averaged specific energy $\vec{\boldsymbol{u}}$: ensembled averaged velocity $\boldsymbol{p}$: ensembled averaged pressure $\boldsymbol{k_{eff}}$: effective thermal conductivity $\boldsymbol{T}$: temperature λ: latent heat of vaporization $\boldsymbol{\dot{m}_{V\to L}}$: condensation liquid phase source term $\boldsymbol{\dot{m}_{L\to V}}$: evaporation liquid phase source term
Fluid	Effective thermal conductivity	Eq. (4)	$k_{eff} = k+\frac{Cp\mu_T}{\mathrm{Pr}_T}$	$\boldsymbol{k}$: two-phase volume fraction averaged thermal conductivity $\boldsymbol{Cp}$: two-phase volume fraction averaged heat capacity $\boldsymbol{\mu_T}$: two-phase volume fraction averaged turbulent viscosity $\boldsymbol{Pr_T}$: turbulent Prandtl number
Solid	Energy	Eq. (5)	$\frac{\partial(\rho_s Cp_s T_s)}{\partial t} = \nabla\cdot(k_s\nabla T_s)$	$\boldsymbol{\rho_s}$: solid density $\boldsymbol{Cp_s}$: solid heat capacity $\boldsymbol{T_s}$: solid temperature
Fluid	Turbulent kinetic energy	Eq. (6)	$\frac{\partial(\rho K)}{\partial t}+\nabla\cdot(\rho K\vec{u}) = \nabla\cdot\left[\left(\mu+\frac{\mu_T}{\sigma_k}\right)\nabla K\right]+G_K-Y_K$	$\boldsymbol{K}$: turbulent kinetic energy $\boldsymbol{\sigma_K}$: turbulent Prandtl number for ω $\boldsymbol{G_K}$: generative term for K due to mean velocity gradients $\boldsymbol{Y_K}$: dissipative term for K due to turbulence
Fluid	Turbulent specific dissipation rate	Eq. (7)	$\frac{\partial(\rho\omega)}{\partial t}+\nabla\cdot(\rho\omega\vec{u}) = \nabla\cdot\left[\left(\mu+\frac{\mu_T}{\sigma_\omega}\right)\nabla\omega\right]+G_\omega-Y_\omega$	$\boldsymbol{\omega}$: turbulent specific dissipation rate $\boldsymbol{\sigma_\omega}$: turbulent Prandtl number for ω $\boldsymbol{G_\omega}$: generative term for ω $\boldsymbol{Y_\omega}$: dissipative term for ω
Fluid	Turbulent viscosity	Eq. (8)	$\mu_T = \frac{\alpha^*(\rho k)}{\omega}$	For the definition of α^* see (ANSYS Inc, 2018)
Fluid	Vapor volume fraction	Eq. (9)	$\alpha_V = 1-\alpha_L$	$\boldsymbol{\alpha_V}$: vapor volume fraction $\boldsymbol{\alpha_L}$: liquid volume fraction
Fluid	Liquid volume fraction	Eq. (10)	$\frac{1}{\rho_L}\left[\frac{\partial(\alpha_L\rho_L)}{\partial t}+\nabla\cdot(\alpha_L\rho_L\vec{u})\right] = \dot{m}_{V\to L}-\dot{m}_{L\to V}$	$\boldsymbol{\rho_L}$: liquid density
Fluid	Two-phase averaged material properties	Eq. (11)	$\psi = \alpha_L\psi_L+(1-\alpha_L)\psi_V$	$\boldsymbol{\psi}$: two-phase volume fraction averaged property $\boldsymbol{\psi_L}$: liquid property $\boldsymbol{\psi_V}$: vapour property

area is discretized with an unstructured mesh with a maximum element size of 0.01 m. Thirty inflation layers (first layer thickness of 1×10^{-4} m and growing rate of 1.1) are added to refine the grid at the interface between the inner tank wall and the fluid (Fig. 2b), where higher gradients are expected. Overall, the CFD domain consists of 7579 control volumes. The "Insulation model domain" is simulated via an MLI degradation model (see Section 2.5), implemented through a User Defined Function (UDF). The two sub-domains are coupled as the fire engulfment boundary condition provided to the "Insultation model domain" is used by the MLI degradation model to calculate the heat flux to the outer surface of the inner tank shell, which in turn represents the boundary condition for the "CFD domain".

2.3. Model set-up

In ANSYS Fluent, the Volume Of Fluid (VOF) model is selected to track gaseous and liquid hydrogen volume fractions in the computational domain and solve the continuity equation (Hirt and Nichols, 1981). The evaporation-condensation mechanism is simulated using the Lee model (Lee, 1980), following previous similar studies (Iannaccone et al., 2021; Scarponi et al., 2024). The saturation temperature curve was implemented as a piece-wise function of the pressure. Above the critical pressure, the saturation pressure is assumed equal to the critical temperature. Since specific experimentally validated data is not available, the default evaporation and condensation frequency values of 0.1 s^{-1} provided in the software were used in the simulation (ANSYS Inc, 2018) as they were shown to give good predictive performance in previous studies addressing similar phase-change and cryogenic conditions (Kangwanpongpan et al., 2023; Liu et al., 2018; Nubli and Wen, 2025). The $k-\omega$ SST model (Launder and Spalding, 1983) is used to model turbulence. The governing equations solved in the CFD simulation are reported in Table 1.

For pressure and phase volume fraction, the PRESTO! (Pressure Staggering Option) and the Geo-Reconstruction discretisation methods are chosen, respectively. The SIMPLEC (Semi-Implicit Method for Pressure Linked Equation) method is selected for the pressure-velocity coupling with no skewness correction. For density, momentum, energy, turbulent kinetic energy, and dissipation rate, second-order discretization schemes are used while the least square cell-based discretisation method is used for gradients. For the transient formulation, a first order implicit scheme was adopted. The time step is case-sensitive. Thus, it should be defined on the basis of a time step independency study. An example is provided in the set-up of the validation test simulation. For the simulations, a baseline time step of 0.01 s is

Table 2
Equations solved for the thermal nodes in the MLI degradation model (Camplese et al., 2024); Subscripts refer to: Se=external shell; N = Nth MLI reflective layer; rl=reflective layer; i = ith MLI reflective layer.

Thermal node	Equation N°	Variable	Equation
S_e	Eq. (13)	T_{S_e}	$\delta_{S_e}\rho_{S_e}c_{p,S_e}\frac{dT_{S_e}}{dt} = \varepsilon_{S_e}(I_R - \sigma T_{S_e}^4) - \frac{1}{\left(\frac{1}{\varepsilon_{S_e}}+\frac{1}{\varepsilon_N}-1\right)}\sigma\left(T_{S_e}^4 - T_N^4\right) - q_{g,Se}$
N	Eq. (14)	T_N	$\delta_{rl}\rho_{rl}c_{p,rl}\frac{dT_N}{dt} = q_{g,Se} + \frac{\sigma\left(T_{S_e}^4 - T_N^4\right)}{\frac{1}{\varepsilon_{S_e}}+\frac{1}{\varepsilon_N}-1} - q_{rl,N}$
i	Eq. (15)	T_i	$\delta_{rl}\rho_{rl}c_{p,rl}\frac{dT_i}{dt} = q_{rl,i+1} - q_{rl,i}$
1	Eq. (16)	T_1	$\delta_{rl,1}\rho_{rl}c_{p,rl}\frac{dT_1}{dt} = q_{rl,2} - q_{rl,1}$

t: time
δ : thickness
ρ : density
c_p : specific heat
T: temperature
ε : emissivity
I_R: incident radiation (see Eq. (12))
σ: Stefann-Boltzman constant (5.67 $\times 10^{-8}$ W m^{-2} K^{-4})
q_g: gas heat transfer (see Eq. (18))
q_{rl} : total heat flux to a reflective layer (see Eq. (17))

chosen.

The default relative and absolute convergence criteria are selected for all the equations (ANSYS Inc, 2018), while under-relaxation factors are chosen following the indications provided by Ustolin et al. (2022).

2.4. Material database and initial conditions

Hydrogen properties are defined with a user-defined database in which specific heat, thermal conductivity, and viscosity are implemented as piecewise linear functions of temperature, based on the data provided by the NIST database (National Institute of Standards and Technology, 2021). The Boussinesq approximation (ρ_{ref} = 63.343 kg m^{-3}, $\beta = 0.036$, for details on the parameters see (ANSYS Inc, 2018)), is used to calculate the density of the liquid phase. The use of a real gas equations of state (e.g., the Peng-Robinson) in the preliminary phase of the work caused convergence issues. Therefore, following the approach proposed in previous studies (Cirrone et al., 2023), the ideal gas equation is used to calculate the vapor density. The initial conditions are defined based on the experimental data of the fire test selected for the model validation (see Section 3.1).

2.5. MLI degradation sub-model

In the present study, the model proposed and validated by Camplese et al. (2024) for MLI reflective layers and glass fiber spacers is used to model the heat transfer through the insulation annular space, accounting for its dynamic thermal degradation. To calculate the heat transferred from the fire to the inner tank wall, the "Insulation model domain" (Fig. 2a) is divided as shown in Fig. 1d. Overall, N+ 2 thermal nodes are considered: N is the number of reflective layers in the MLI and the two additional layers represent the tank inner and outer shells, S_i and S_e respectively. For each node, a thermal balance is written and solved to obtain its temperature over time.

The boundary condition provided to the model is the incident radiation I_R to the tank outer shell, calculated by Eq. (12),

$$I_R = \sigma T_{BB,fire}^4 \tag{12}$$

where σ is the Stefan-Boltzmann constant (5.67 $\times 10^{-8}$ W m^{-2} K^{-4}) and $T_{BB,fire}$ is the black body temperature of the fire in K. The equations solved for the $N + 2$ thermal nodes are summarized in Table 2, where nodes 1 and N refer to the reflective layers facing the inner and outer shells, respectively.

The model relies on a modified version of the layer-by-layer approach proposed by Mcintosh (1994) to account for the heat transfer between two adjacent reflective layers. The total heat flux ($q_{rl,i}$) is calculated with Eq. (17), accounting for the thermal radiation ($q_{rad,i}$), solid conduction ($q_{s,cond,i}$) and gas heat transfer ($q_{g,i}$). The latter contribution is represented by convection or conduction depending on the vacuum pressure within the insulation system and the fluid-dynamic regime (Eq. (18)). Specifically, $q_{g,i}$ is calculated with the Sherman-Lees relation (Liu and Lees, 1961; Sherman, 1963) for conduction ($q_{g,cond,i}$) when the Grashof number (Gr) is below 2860 (Xie et al., 2010). For higher G_r values, $q_{g,i}$ is obtained based on the transition to convective heat transfer ($q_{g,conv,i}$), calculated according to Xie et al. (2010). This approach allows to apply the model in all relevant pressure ranges, from high vacuum to loss of vacuum conditions.

$$q_{rl,i} = q_{rad,i} + q_{s,cond,i} + q_{g,i} = \frac{\sigma(T_i^4 - T_{i-1}^4)}{\frac{1}{\varepsilon_i}+\frac{1}{\varepsilon_{i-1}}-1} + \frac{f_i^2 k_s}{D_x}(T_i - T_{i-1}) + q_{g,i} \tag{17}$$

$$q_{g,i} = \begin{cases} Gr < 2860, \quad q_{g,i} = q_{g,cond,i} = \left[\frac{D_x}{k_g} + \frac{2-\theta}{\theta}\times\sqrt{\frac{\pi MT}{\left(1+\frac{\zeta}{4}\right)P}}\right]^{-1} \times (T_i - T_{i-1}) \\ Gr \geq 2860, \quad q_{g,i} = q_{g,conv,i} = \frac{Nuk_g}{D_x}(T_i - T_{i-1}) \end{cases} \tag{18}$$

Where f_i is the relative solid fraction (i.e., the ratio of the density of the spacer to the density of the fiber material), k_s is the solid thermal conductivity of the spacer parent material (i.e., glass fiber) in W m^{-1} K^{-1}, D_x is the spacer thickness in m, k_g is the gas thermal conductivity in W m^{-1} K^{-1}, θ is the accommodation factor, M is the molecular weight of the gas in kg mol^{-1}, ζ is the atomic degrees of freedom in the gas (2 for air and nitrogen), and P is the pressure in Pa. To account for the gradual high-temperature degradation of MLI materials, the method proposed by Camplese et al. (2023) and Hajhariri et al. (2025) for MLI systems with aluminium reflective layers and glass fiber spacers is applied.

In the thermal balance for the node corresponding to the external shell (see Eq. (13) of Table 2), the heat flux to the outermost intact MLI layer is due to radiation and conduction only, since a vacuum gap is present between the external shell and the MLI system.

The thermal balance for the inner shell is not solved in the MLI degradation model as the inner shell temperature (T_{S_i}) is directly calculated within the "CFD domain". The same parameter is required as

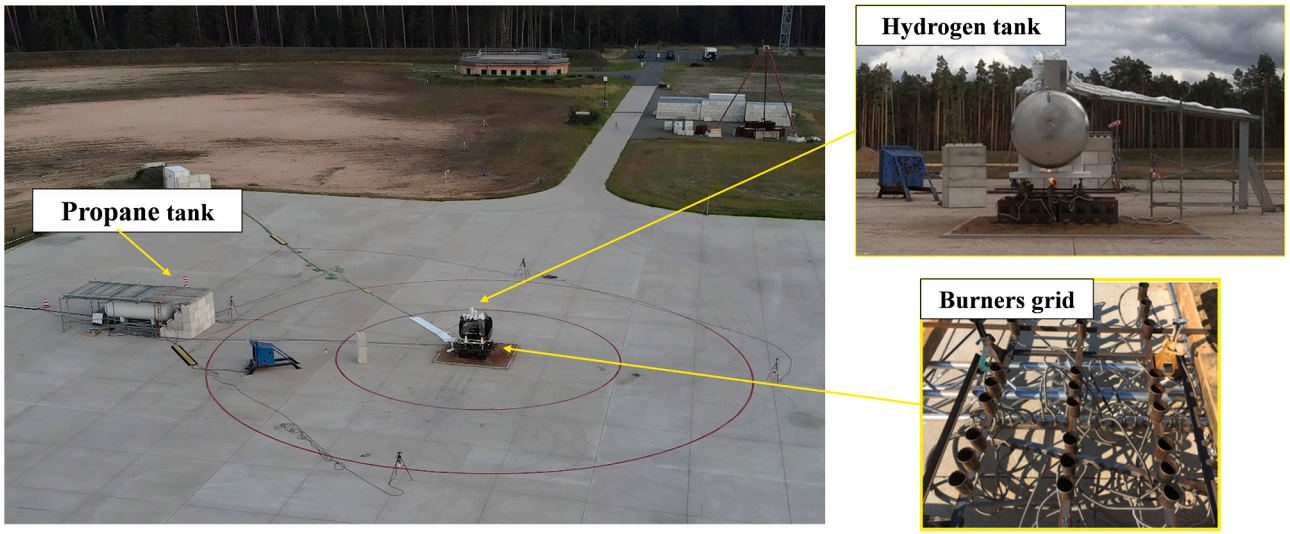

Fig. 3. Experimental set-up of the fire test used for model validation.

Table 3
Features of the cryogenic tank involved in the experimental fire test used for model validation.

Parameter	Value
Inner volume (m^3)	1
Inner shell thickness (m)	0.003
Outer shell thickness (m)	0.004
Insulation thickness (m)	0.21
Vacuum pressure (bar)	0.0003
Number of MLI layers	20
Filling degree (%)	35–40
Mass of liquid hydrogen (kg)	25–30
Liquid temperature (K)	22
Vapour temperature (K)	32

an input to the MLI degradation model. It is worth mentioning that in the model proposed by Camplese et al. (2024) at each iteration a single value of the inner shell temperature (T_{S_i}) is considered as an input to the model, neglecting the heat transfer in the direction parallel to the wall. In this study, the minimum shell temperature is selected to this purpose. This choice is conservative since it maximizes the thermal gradient (and thus the heat flux) between the outer and inner shell.

The MLI degradation sub-model is implemented and solved in the CFD simulation through a UDF, which provides the heat flux profile on the outer surface of the internal shell. This is calculated with Eq. (19), as follows:

$$q_{Si} = q_{rl,1} = \begin{cases} T_1 < 933.45\,K, & \dfrac{\sigma\left(T_1^4 - T_{Si}^4\right)}{\dfrac{1}{\varepsilon_1}+\dfrac{1}{\varepsilon_{Si}}-1} + \dfrac{{f_1}^2 k_s}{D_x}\left(T_1 - T_{Si}\right) + q_{g,1} \\ T_1 \geq 933.45\,K, & \dfrac{\sigma\left(T_{Se}^4 - T_{Si}^4\right)}{\dfrac{1}{\varepsilon_{Se}}+\dfrac{1}{\varepsilon_{Si}}-1} + q_{g,Se} \end{cases} \quad (19)$$

The combination of the CFD simulation with the MLI degradation model will be referred to as the DEG model or, more simply, DEG, in the following.

3. Model validation

3.1. Experimental test and specific assumption introduced in the simulation

The validation of the model proposed in this study has been carried out comparing the model results with the experimental outcomes of a fire test carried out on an LH_2 storage tank as part of the SH_2IFT (Safe Hydrogen Fuel Handling and Use for Efficient Implementation) project at the Bundesanstalt für Materialforschung und prüfung (BAM). The experimental set-up is shown in Fig. 3. During the test, the catastrophic rupture of the tank resulted in a LH_2 BLEVE. The LH_2 tank used in the test was a 1 m^3 double-walled insulated vessel entirely made of low-temperature resistant stainless steel (X5 CrNi 18–10). The vessel was oriented horizontally and contained around 25–30 kg of liquid hydrogen (filling degree of 35–40 %). At the beginning of the test, hydrogen pressure was 3.81 bar, and the two thermocouples placed in the bulk of the liquid and vapor space (one in each phase) read 22 K and 32 K, respectively. The insulation system, positioned inside the 0.21 m gap between the inner and the outer tank shells, consisted of a multi-layer insulation under high vacuum (initial vacuum pressure of 0.3 mbar). The MLI consisted of 20 reflective layers. The features of the tank are summarized in Table 3.

The fire engulfment was generated using 36 propane burners positioned under the tank. The pressure relief valve was remotely activated when the inner pressure reached 48.54 bar. The catastrophic rupture of the tank was observed 62 min after the beginning of the fire exposure. Further details on the test are reported in Ødegård et al. (2022).

In order to simulate the experimental test, specific assumptions have been introduced in the model concerning the flame temperature and the MLI.

The flame temperature was not measured during the SH_2IFT test. However, in the experimental setup, a thermocouple was positioned at the centre of the tank bottom surface. Since this area is the closest to the burners grid, the recorded measurements are used to define the flame black body temperature. Experimentally, the surface temperature was in the range of 1000 – 1100 K. These two extreme values are used for $T_{BB,fire}$ (Eq. (12)) in the simulations.

The available experimental temperature values for the liquid are affected by a high uncertainty. Only one thermocouple was installed in the vessel, and its exact position is not reported in the experimental documentation. Since the liquid is not mechanically stirred, significant thermal stratification may occur, and the measured value (22 K) is likely representative of a local temperature near the wall rather than of the bulk liquid. For this reason, the experimental temperature reading was not used directly. Instead, the average initial liquid temperature was estimated from the initial gas pressure, assuming thermodynamic equilibrium between the liquid and vapour phases. The saturation temperature at the initial pressure of 3.81 bar (25.84 K) was therefore imposed as the initial temperature for both phases.

Table 4
Features of the meshes used for the grid sensitivity analysis.

Mesh ID	Element size (cm)	Number of control volumes
M0	1	7579
M1	0.5	17524
M2	0.25	69662

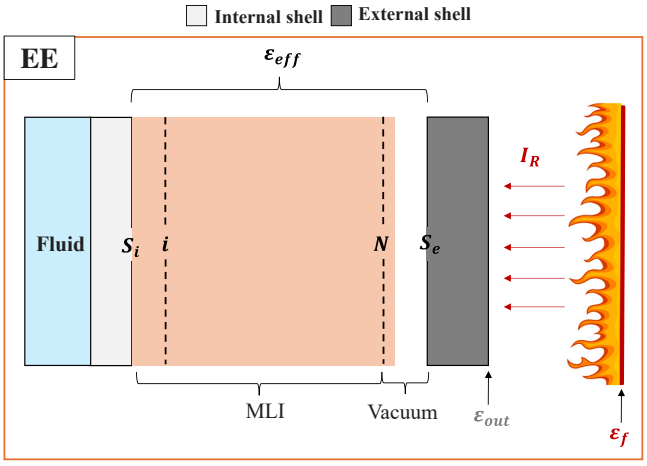

Fig. 4. Scheme of the insulation annular space according to the procedure described in (ASTM International, 2019); MLI = Multi-layer insulation.

The experimental value of the initial filling degree is also affected by a high uncertainty, ranging between 35 % and 40 %. The highest value (40 %) was selected in the simulations to obtain a conservative estimate of tank internal pressure, since a higher filling degree leads to more severe tank pressurization (Moodie et al., 1988; Scarponi et al., 2024).

While the number of layers and the type of the MLI were determined by the analysis of the vessel fragments following the experimental test, all the other characteristics of the MLI insulation used in the model were derived from literature data concerning the MLI type used in the vessel, since the specific values for the material used in the experimental test are unknown. Specifically, a MLI with unperforated aluminium reflective layers (thickness = 6 μm) interleaved by glass fleece spacers (thickness = 455 μm) has been considered in the simulations. A value of 0.04 has been selected for the emissivity of the MLI reflective layers (ε_i in Eq. (17)), considering the highest among the values available in the literature (Jiang et al., 2021; Wang et al., 2016). A value of 0.27, measured by Eberwein et al. (2023) in post fire-like test conditions, is used for the emissivity of the external wall (ε_{S_e} in Eq. (13) and Eq. (19)). The properties of the X5 CrNi 18–10 stainless steel (density = 7900 kg m^{-3}, thermal conductivity = 15 W m^{-1} K^{-1}, specific heat capacity = 500 J kg^{-1} K^{-1}) (Altair Engineering Inc.., 2025) are used for the inner shell of the tank. The value of the other MLI properties required to close the set of equations of the DEG model (see Section 2.5) are obtained from (Hajhariri et al., 2024).

The CFD simulations of the experimental test were carried out until the internal pressure reached the maximum value recorded during the experimental test (around 50 bar).

The grid independency of the results has been tested using two finer meshes whose features are summarized in Table 4. Time-step independence of the results has been assessed by repeating the simulations with two additional time steps obtained by doubling (0.02 s) and halving (0.005 s) the baseline value. The details of the grid and time step independence assessment are reported in Appendix A.

3.2. Comparison with a state-of-the-art sub-model for MLI degradation

As mentioned previously, state-of-the-art models proposed for the fire exposure of insulated cryogenic LH_2 tanks do not include a detailed simulation of the insulation behaviour under high thermal loads, but rather introduce a pre-defined insulation performance, assuming highly empirical insulation thermal parameters (e.g., thermal conductivity or effective emissivity). The MLI degradation sub-model implemented in this study significantly differs from these approaches, as it captures the dynamic variation of the insulation thermal performance, without leaving the MLI characterization to the analyst choice.

Table 5
Simulations carried out in the present study: validation case and benchmarking cases.

Case ID	Purpose	MLI performance	Number of layers (N)	Fire black body temperature (K)
DEG_1100 *	**Validation**	**Detailed model** - Camplese et al. (2024)	**n.a.**	**1100**
DEG_1000	Benchmarking	Detailed model - Camplese et al. (2024)	n.a.	1000
EE_W_1100	Benchmarking	ASTM model – Undegraded MLI	20	1100
EE_W_1000	Benchmarking	ASTM model – Undegraded MLI	20	1000
EE_P_1100	Benchmarking	ASTM model – Partially degraded MLI	10	1100
EE_P_1000	Benchmarking	ASTM model –Partially degraded MLI	10	1000
EE_D_1100	Benchmarking	ASTM model - Completely degraded MLI	0	1100
EE_D_1000	Benchmarking	ASTM model - Completely degraded MLI	0	1000

* validation cases

To benchmark the predictive capability of the proposed sub-model against the state-of-the-art approaches used in previous CFD approaches, a comparison with the adaptation of the method described in the C749/C740M-13 ASTM standard (ASTM International, 2019) is carried out. In the standard, the procedure to calculate the MLI effective emissivity in ideal conditions (i.e., free floating reflective layers of very low emittance and of infinite extent) is proposed. The method is adapted according to the procedure proposed by Howell et al. (2010) for MLI systems between two walls in order to include the inner and outer tank shells. Considering the schematization of the insulation domain as shown in Fig. 4, the effective emissivity (ε_{eff}) is calculated as in Eq. (20):

$$\frac{1}{\varepsilon_{eff}} = \frac{1}{\varepsilon_{S_i}} + \frac{1}{\varepsilon_{S_e}} - 1 + \sum_{i=1}^{N} \left(\frac{1}{\varepsilon_{i,S_i}} + \frac{1}{\varepsilon_{i,S_e}} - 1 \right) \tag{20}$$

where the subscripts S_i and S_e refer respectively to the surface of the inner and outer walls in contact with the insulation, N is the total number of reflective layers of the MLI, and ε_{i,S_i} and ε_{i,S_e} are respectively the emissivities of the i^{th} layer oriented towards the inner and the outer tank wall. The heat flux to the inner tank shell is calculated as in Eq. (21) (ANSYS Inc, 2018):

$$q = \varepsilon_{eff}(I_R - \sigma T_w^4) \tag{21}$$

where T_w is the temperature of the outer surface of the tank inner wall in K.

The emissivity of the MLI layers and external wall (ε_{i,S_i}, ε_{i,S_e}, and ε_{S_e} in Eq. (20)) are the same as those used in the DEG model (0.04 and 0.27, respectively). In the case of the inner wall (ε_{S_i} in Eq. (20)), a value of 0.27 is chosen based on the measurements conducted by Eberwein et al. (2023) on AISI 316 L stainless steel at ambient conditions.

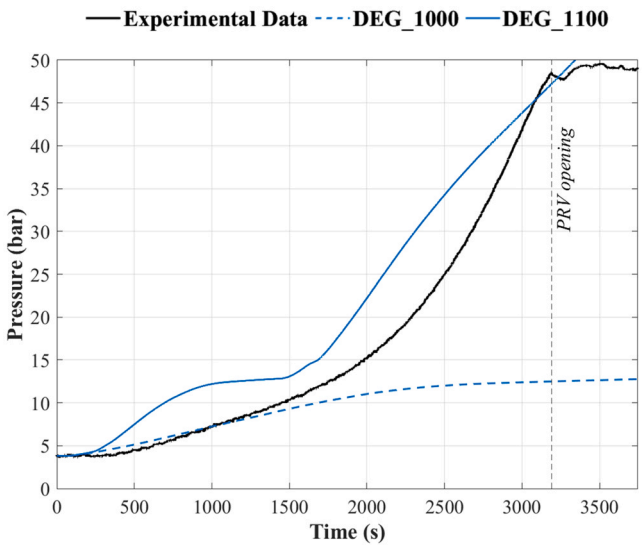

Fig. 5. Comparison of the experimental pressure with the simulations obtained from the DEG model (see Table 5 for the key to simulation runs); PRV: pressure relief valve.

The effective emissivity obtained considering the best-case scenario of a perfectly working MLI (i.e., all the 20 reflective layers remain active during the fire exposure) is 0.001. However, as previously mentioned, some degradation was observed during experimental tests. Therefore, two additional cases are considered to simulate the degradation phenomena. First, the initial number of layers is halved to account for the MLI partial degradation, obtaining an effective emissivity of 0.002. In the third case, the worst-case scenario of complete MLI degradation is assumed, considering that all the layers are immediately degraded at the beginning of the test. In this case, the effective emissivity is 0.44. The combination of the CFD simulation with the method described above (i.e., effective emissivity) will be referred to as the EE model (EE in the following).

Table 5 summarizes all the cases considered in this analysis with both the DEG and EE models.

4. Results

4.1. Validation results

The grid and time step sensitivity analysis demonstrated the grid and time step independence of the results (see Appendix A). Thus, in the following sections the results obtained with the M0 mesh and the baseline time step of 0.01 s are presented.

The tank self-pressurization calculated with the DEG model is compared with the experimental data of the SH_2IFT fire test in Fig. 5.

The outcomes of the simulation highlight the key role of the flame temperature in the prediction of the pressure build-up inside the cryogenic tank. The best prediction of the pressure relief valve activation time (~ 3180 s) is obtained in the DEG_1100 case, with a relative error of 2.4 %. When a lower fire black body temperature is considered (DEG_1000 case), the simulation fits well the experimental data for the first 1250 s. Afterwards, the calculated pressure curve shows a considerable deviation from measured values. The reason for such a large difference between the outcomes of the DEG_1100 and DEG_1000 simulations is due to the behaviour of the insulation system which is very different between the two cases, as shown in Fig. 6a. More specifically, in the DEG_1000, two layers are destroyed within about 600 s from the beginning of the fire (blue dotted line in Fig. 6a) test while a significantly faster degradation occurs considering a higher fire temperature, as in the DEG_1100 simulation, leading to the destruction of 15 layers within 400 s (blue continuous line in Fig. 6a).

Actually, the degradation process within the MLI system in the DEG model is correlated with the temperature evolution of each single layer. The results for five representative layers (1st, 5th, 10th, 15th, and 20th layer) are illustrated in Fig. 6b for the case DEG_1000 and in Fig. 6c for the case DEG_1100. These results are in agreement with the experimental evidence produced by Eberwein et al. (2024b) and Hajhariri et al. (2025), who observed the partial degradation of the aluminium-based MLI when exposed to temperatures similar to those considered in the present study.

As shown in Fig. 7 (panels a to c), the possible presence of a temperature stratification in the fluid during the fire exposure is predicted by the model. In the DEG_1100 case, vertical temperature gradients are established during the fire exposure, with temperature peaks around 350 K in the vapour phase. Differently, in the DEG_1000 case, the fluid temperature is homogeneous in the vertical direction, showing negligible stratification. Relevant differences among the two model runs are obtained also when considering the liquid phase temperature and level. As shown in Fig. 7 (panels d to f), although the liquid temperature is almost the same at the end of the simulations (around 33 K), the heating velocity of the liquid phase is different. In the DEG_1000 case, the final liquid temperature is approached gradually after 3400 s, while in the DEG_1100 case it is reached after 1500 s due to the quick breakdown of the reflective layers and the consequent reduced shielding effect of the insulation. The liquid level is constant in the DEG_1000 case, while almost no liquid remains in the vessel at the end of the DEG_1100 simulation. It is worth noting that supercritical fluid conditions are obtained in the DEG_1100 case after approximately 1800 s from the beginning of the simulation.

4.2. Benchmarking with conventional modelling approaches for MLI degradation

In the following, the results of the CFD model integrating the MLI degradation sub-model are compared with those obtained using a conventional modelling approach, based on an empirical value of the thermal conductivity (EE model, see Section 3.2)

The pressure build-up of the cryogenic tank predicted with the EE model considering the lowest and highest fire black body temperatures is shown in Fig. 8. It is evident that the EE approach fails in reproducing the test outcome, regardless of the insulation configuration and flame temperature assumed. On the one hand, when partial or no degradation of MLI is considered in the EE model (EE_W and EE_P curves), the pressure increase during the fire exposure is negligible. On the other hand, when a total degradation of MLI is assumed, (EE_D curves), an unrealistically fast pressurization is predicted (i.e., more than 50 bar in 500 s), leading to the almost immediate opening of the relief valve. The temperature assumed for the fire has a limited effect on the results.

Significant discrepancies are observed between the pressure curves obtained with the EE model (Fig. 8) and the DEG model (Fig. 5). These results reflect the differences in the heat flux entering the CFD domain – specifically, the heat flux to the inner tank wall – obtained in the different simulations. The heat flux to the tank inner wall depends on the incident radiation (I_R) to the tank outer shell, calculated by Eq. (12), and is governed by the selected model used to reproduce the insulation behaviour. In turn, the incident radiation is determined by the fire black body temperature ($T_{BB,fire}$). When $T_{BB,fire} = 1000$ K, the I_R is 56.7 kW m^{-2}, and increases by 47 % (i.e., to 83 kW m^{-2}) when $T_{BB,fire} = 1100$ K. Fig. 9 shows the heat flux received by the inner tank shell calculated with the different models for both the fire temperatures.

Fig. 9a shows the results obtained using the EE model. When the insulation is intact, the heat received by the tank is lower than 10 W m^{-2} (green curves in Fig. 9a), causing a negligible pressurization. For the case of partial degradation of the insulation (yellow curves in Fig. 9a), the heat flux to the tank is around 10^2 W m^{-2}, still leading to almost no

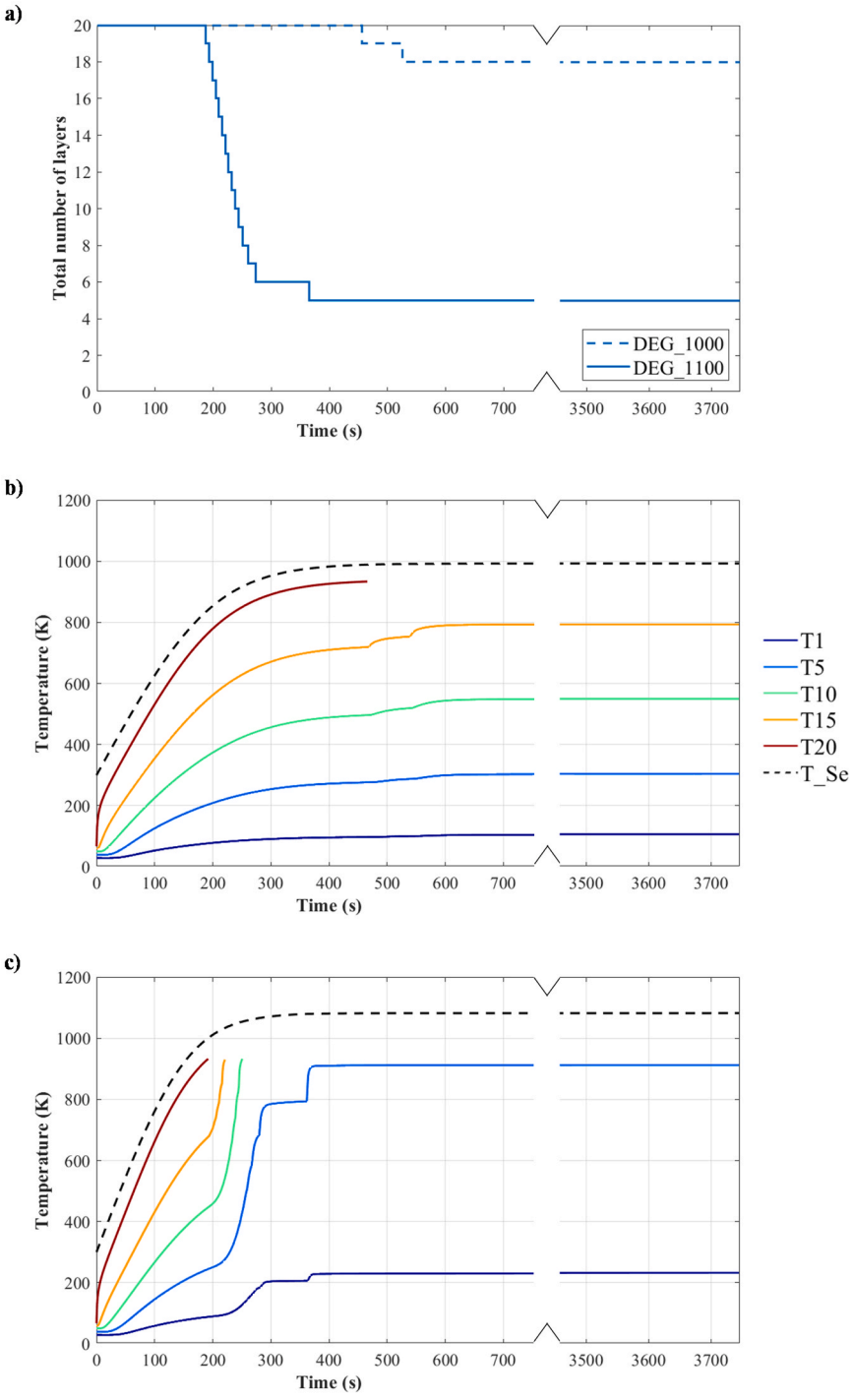

Fig. 6. a) Number of degraded MLI layers in the simulation of the fire test; b) Temperature profiles of the 1st (T1), 5th (T5), 10th (T10), 15th (T15), 20th (T20) reflective layers of the MLI insulation and external shell (T_{S_e}) for the DEG_1000 case and c) for the DEG_1100 case (see Table 5 for the key to simulation runs).

pressure build-up. Conversely, when the insulation is assumed to be completely degraded, the heat flux reaches values on the order of 10^4 W m^{-2} (red curves in Fig. 9a), leading to the rapid pressure rise observed in Fig. 8.

When the fire temperature $T_{BB,fire}$ is increased from 1000 K to 1100 K, a consistent increase is present in the heat flux curves across all three insulation degradation scenarios. The shift is uniform and directly results from the EE model formulation, where the heat flux is proportional to the incident radiation via the effective emissivity (ε_{eff}). Since I_R increases by 47 % with the 100 K rise in $T_{BB,fire}$, the heat flux to the inner shell increases by the same percentage, regardless of the insulation state or the specific value of ε_{eff}.

When the MLI degradation is simulated using the DEG model, the influence of $T_{BB,fire}$ is lower. Actually, the DEG model incorporates a more detailed physics of the phenomena, that makes the heat flux response dependent on the state of the insulation. As a result, the effect of increasing $T_{BB,fire}$ is less uniform and cannot be captured by a simple scaling factor, reflecting the more complex heat transfer mechanisms involved. The heat fluxes predicted by the DEG model (Fig. 9b) are of the same order of magnitude across both fire temperature scenarios, but they exhibit a markedly stronger dependence on $T_{BB,fire}$ compared to the EE results. Specifically, the peak heat flux increases from approximately

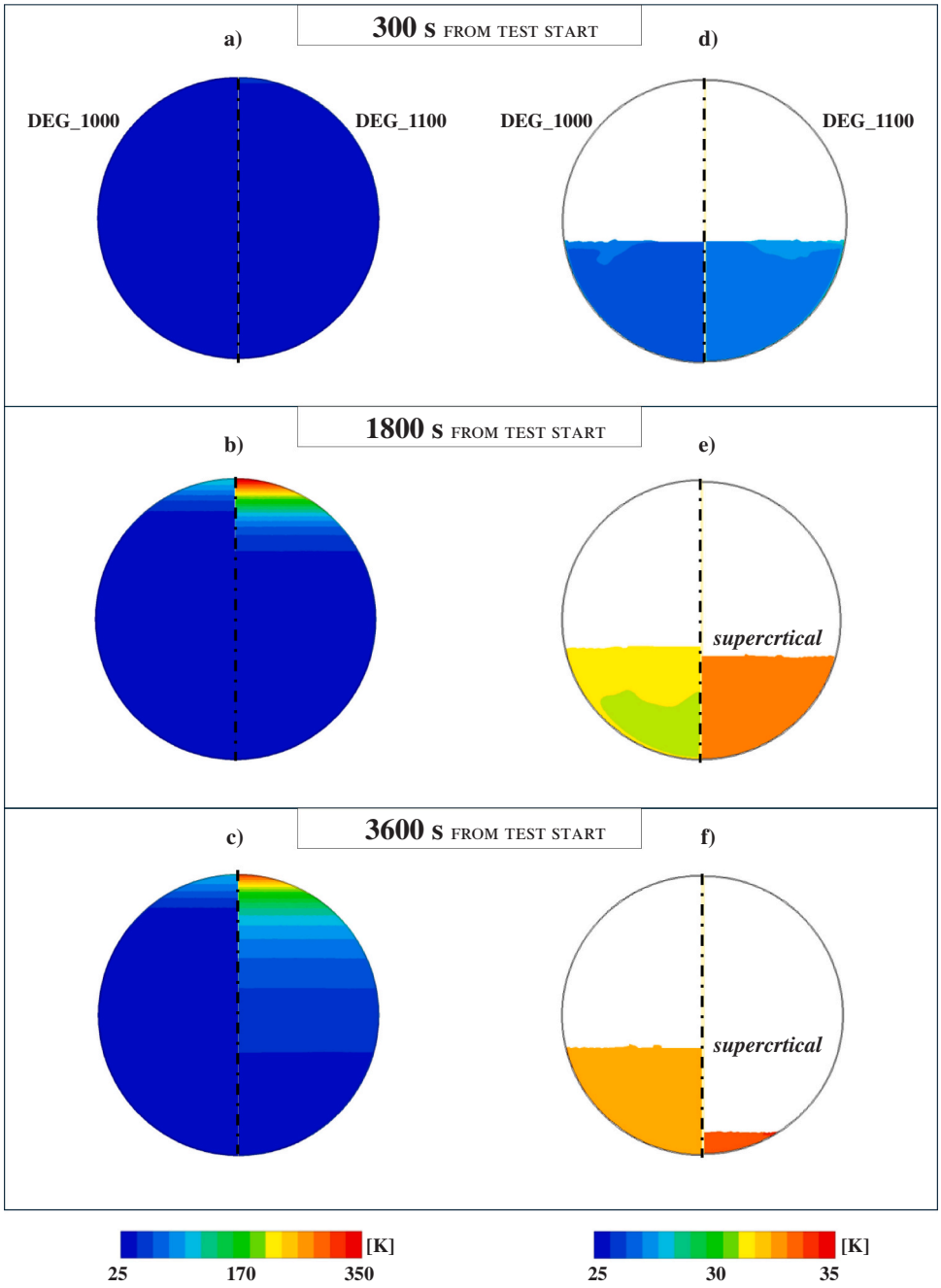

Fig. 7. Values calculated in the DEG_1000 and DEG_1100 CFD model runs for the fluid temperature after a) 300 s, b) 1800 s, and c) 3600 s from the beginning of the fire test, and for the liquid temperature and level after d) 300 s, e) 1800 s, and f) 3600 s from the beginning of the fire test (see Table 5 for the key to simulation runs).

1 W m^{-2} for DEG_1000 to about 3.3 W m^{-2} for DEG_1100, corresponding to a 230 % increase (much higher than the 47 % registered for the EE model). The higher sensitivity in the DEG model reflects its more complex handling of temperature and heat flow dynamics, and of the degradation of the insulation, which are not directly proportional to fire temperature changes.

It should be further remarked that a relevant difference is present when comparing the time dependence of the heat flux predicted by the EE and DEG models. While this is constant in the EE models, the DEG model captures a more realistic transient behaviour: the heat flux increases over time as the insulation layers heat up and undergo thermal degradation. This progressive breakdown of the insulation – explicitly accounted for in the DEG model but not in the EE model – is a primary factor in determining the higher sensitivity of the DEG model to fire temperature.

5. Discussion

The results of the validation case show that the 2D modelling approach is able to reproduce with sufficient accuracy the experimental data. In the simulations, the geometry of the real cryogenic tank used in the reference experiment was simplified to half of the tank cross-section, resulting in a 2D symmetric configuration (1D for the heat-transfer model of the insulation). This choice introduces inherent limitations, particularly regarding the representation of internal three-dimensional fluid motion and localized geometric effects. However, for safety assessments of medium-size cryogenic storage tanks exposed to static, fully engulfing fires (i.e., the worst-credible scenario typically employed

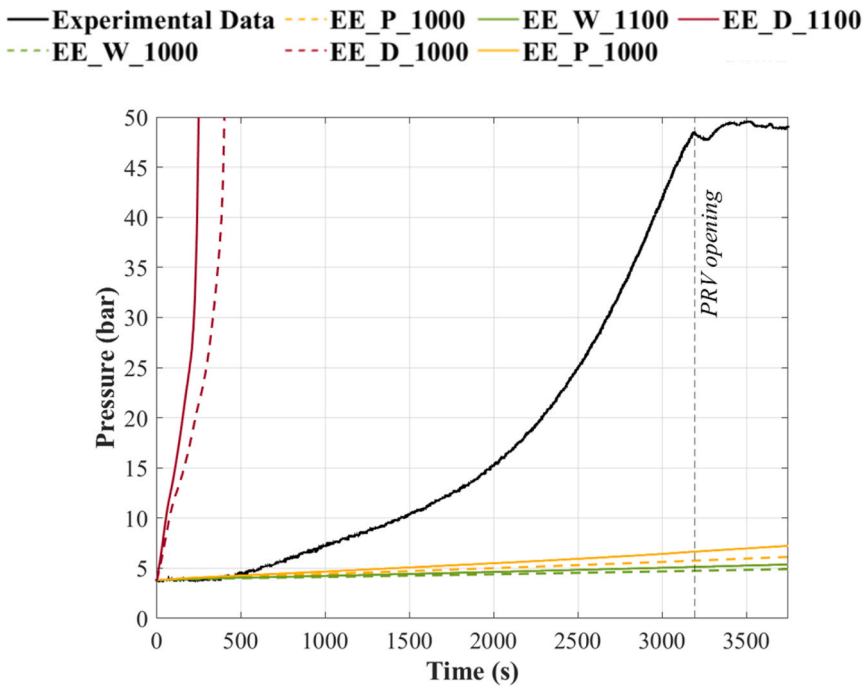

Fig. 8. Comparison of the pressure curves obtained from the CFD simulations using the EE model to reproduce the behaviour of the insulation with the experimental data considering a fire black body temperature of a) 1000 K and b) 1100 K; PRV = pressure relief valve (see Table 5 for the key to simulation runs).

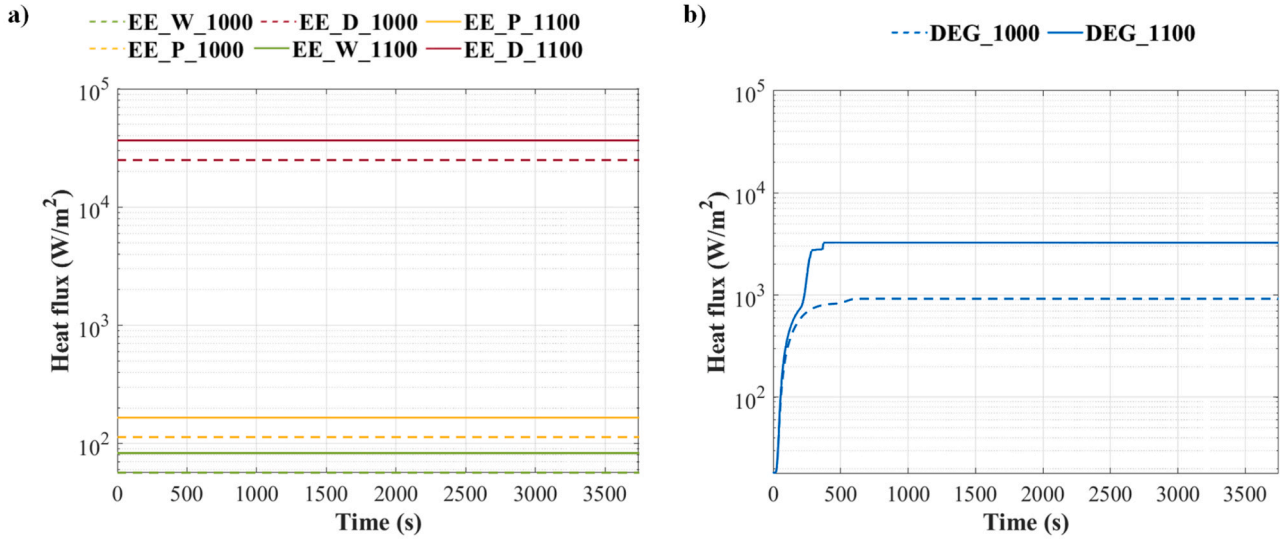

Fig. 9. Heat fluxes predicted at the outer surface of the inner tank shell using either the a) EE model and b) DEG model (see Table 5 for the key to simulation runs).

in industry and in process safety relevant literature), the 2D assumption is widely adopted (Aydemir et al., 1988; Beynon et al., 1988; Birk et al., 2013; Chen and Lin, 1999; Gong et al., 2004; Graves, 1973b; Hadjisophocleous et al., 1990b; Hulsbosch-Dam et al., 2017; Hunt and Ramskill, 1985; Shebeko et al., 2000; Sumathipala et al., 1992). Coherently with the results obtained, under these conditions, previous studies have reported only minor differences between 2D and 3D simulations (Scarponi et al., 2019), supporting the suitability of the present approach for capturing the dominant heat-transfer mechanisms and providing conservative estimates of tank response.

A full 3D model would increase geometric fidelity and becomes essential when the assumption of uniform flame engulfment is not credible (e.g., large tanks or strongly directional fires). However, such model requires a detailed knowledge of fire dynamics (such as spatial flame coverage and asymmetry) which is rarely available in experiments, and it entails a substantially higher computational cost. Even with the simplified 2D geometry, the simulations performed here required approximately three days (EE model) to one week (DEG model) on a 16-core Intel® Core™ i9–9940X. Extending the domain to a full 3D representation, where the simulated volume would increase by more than three orders of magnitude, would lead to prohibitive runtimes and would limit applicability in industrial risk-assessment contexts where timely evaluations are essential.

In light of these constraints, the 2D approach adopted here represents a pragmatic compromise between fidelity and computational feasibility. Future work will focus on exploiting the high-fidelity results of the present model to support reduced-order or hybrid strategies capable of capturing key three-dimensional effects at a fraction of the

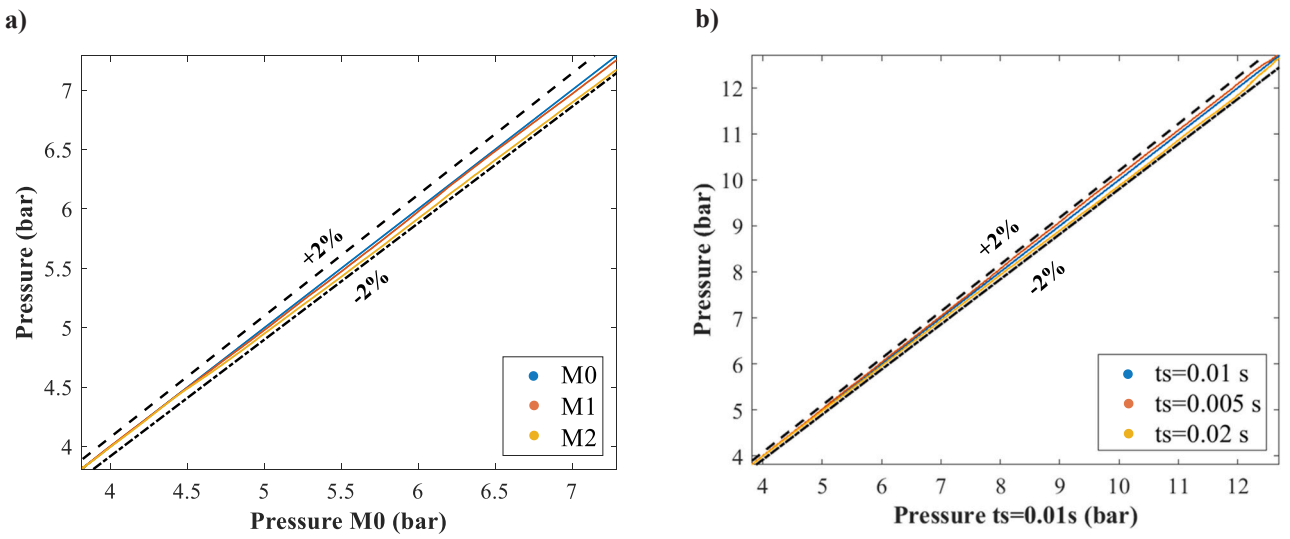

Fig. 10. a) Parity plot with the results of the grid independence study for the three meshes M0 (element size = 1 cm), M1 (element size = 0.5 cm), and M2 (element size = 0.25 cm); b) Parity plot with the results of the time step independence study for time steps (ts) of 0.01, 0.005 and 0.02 s.

computational cost.

When considering the simulation of the insulation layer, the comparison of the model outcomes with the results of a full-scale experimental fire test evidence that the DEG model is suitable to simulate with a sufficient accuracy the full fire engulfment of a LH_2 storage tank insulated with an MLI system. The comparison with experimental data shows that the model correctly captures the thermal and fluid dynamic behaviour of the tank under the intense fire load from engulfing fire scenarios with reasonable accuracy.

The results of the benchmarking of the proposed model with a conventional approach, based on the use of an empirical constant thermal emissivity value (i.e., the EE model), highlight the importance of dynamically reproducing the MLI degradation to accurately predict the tank self-pressurization during fire exposure. In this sense, the proposed model represents a significant advancement with respect to the current state-of-the-art.

However, several limitations are still present in the proposed modelling approach. A key factor influencing the model results is the fire temperature. As mentioned in Section 3.1, the values of the fire black body temperature selected in this study are obtained from a thermocouple positioned on the tank bottom surface. Although this location is the closest to the burner array, significant uncertainty remains regarding the actual average flame temperature. The sensitivity of the model to the fire black-body temperature therefore represents a key factor of uncertainty. This is particularly critical during validation, where reproducing the actual experimental heat flow is crucial, while direct flame temperature measurements are often unavailable in most large-scale experimental set-ups. Improved fire temperature characterization, for example using directional flame thermometers (Bradley et al., 2021), would reduce this uncertainty and improve the results of the CFD simulations. When predictive applications of the model are aimed at, the fire black body temperature is specified by the analyst, but it remains a critical assumption and its influence on the results should be explored in detail through sensitivity or scenario analysis.

A further issue concerns the effect of the variation in the insulation properties assumed in the MLI degradation model. A high uncertainty affects the variation of such properties during the experimental run, and direct experimental measurement is challenging. However, a sensitivity analysis performed by Camplese et al. (2025) showed that ±10 % variation in the input properties leads to variations in the model outputs always lower than 5 %. In particular, the number and emissivity of the layers were identified as the two most influential parameters. In the validation case considered in the present study, the number of layers was derived directly from the experimental data and therefore does not contribute to uncertainty. By contrast, the experimental emissivity remains unknown. Nevertheless, the values adopted in the simulation are derived from experimental data reported in the literature for the same type of insulation used in the test. Thus, limited deviations are reasonably expected.

It is also worth remarking that the DEG model does not consider the loss of vacuum in the insulation annular space: the initial vacuum pressure is provided as an input and is not updated during the simulation. Even if the simulation of these aspects remain challenging due to their case-specific nature (Camplese et al., 2024), the addition of the effect of vacuum loss, also considering the formation of gaseous MLI decomposition products and their possible condensation on the inner tank wall, may further increase the accuracy of the model.

6. Conclusions

A 2D CFD model integrated to an innovative dynamic sub-model for MLI degradation has been developed for the simulation of fire engulfment scenarios involving LH_2 storage tanks insulated with MLI. Validation against experimental data from a full-scale fire test confirms the model capability to reproduce the pressurization of the tank in both subcritical and supercritical regimes with reasonable accuracy. Moreover, the comparison with a conventional simplified state-of-the-art submodel for MLI degradation demonstrates the significant increase in the accuracy of the proposed approach, proving the necessity of adopting detailed modelling tools for both the fluid behaviour and the thermal degradation of the insulation when predicting the pressure build-up of cryogenic storage tanks. Simplified static approaches are shown to be inadequate, in particular in scenarios where the insulation performance is compromised. Furthermore, the analysis highlights the strong influence of the fire temperature on the tank pressure build-up, especially in the presence of the degradation of the insulation, highlighting the importance of an accurate fire characterization in future experimental and modelling efforts.

The results evidence that a significant advancement has been obtained by combining CFD modelling with an innovative MLI degradation sub-model into a unified tool for LH_2 storage safety and integrity assessment. The proposed model provides valuable insights for the design and assessment of cryogenic tanks exposed to intense fire scenarios, offering a foundation for the development of effective emergency response strategies and mitigation measures.

CRediT authorship contribution statement

Alice Schiaroli: Writing – original draft, Methodology, Investigation, Data curation, Conceptualization. **Davide Camplese:** Writing – original draft, Methodology, Investigation, Data curation, Conceptualization. **Valerio Cozzani:** Writing – review & editing, Validation, Supervision, Methodology, Investigation, Conceptualization. **Robert Eberwein:** Validation, Methodology, Conceptualization. **Federico Ustolin:** Writing – review & editing, Validation, Supervision, Methodology, Conceptualization. **Giordano Emrys Scarponi:** Writing – review & editing, Validation, Methodology, Investigation, Conceptualization.

Declaration of Competing Interest

The authors declare that they have no known competing financial interests or personal relationships that could have appeared to influence the work reported in this paper.

Acknowledgments

This work was undertaken as part of Project “Network 4 Energy Sustainable Transition”, PE00000021, CUPJ33C22002890007 funded by the Italian Ministry of University and Research under the National Recovery and Resilience Plan, Misson 4, Component 2, Investment 1.3, NextGenerationEU. This work was undertaken as part of the research projects Safe Hydrogen Fuel Handling and Use for Efficient Implementation (SH2IFT) and Safe Hydrogen Fuel Handling and Use for Efficient Implementation 2 (SH2IFT-2), and the authors would like to acknowledge the financial support of the Research Council of Norway under the ENERGIX program (Grant No. 280964 and Grant No. 327009, respectively.). This work was undertaken as part of the ELVHYS project No. 101101381 supported by the Clean Hydrogen Partnership and its members. UK participants in Horizon Europe Project ELVHYS are supported by UKRI gran numbers 10S063519 (University of Ulster) and 10070592 (Health and Safety Executive). Funded by the European Union Views and opinions expressed are however those of the author(s) only and do not necessarily reflect those of the European Union or Clean Hydrogen JU. Neither the European Union nor the granting authority can be held responsible for them.

Appendix A. Grid and time step sensitivity

The grid and time step independence of the model results is assessed considering the case DEG_1000. For the grid independence, the three meshes described in Table 4 are used. The outcomes are shown in Fig. 10a in terms of inner tank pressure. Given the high computational time required by the simulations (around one week with the coarser mesh M0), the results are shown for the first 1000 s. Overall, the difference between the pressure curves obtained with the coarser mesh and the refined ones (M1 and M2) is lower than 2 %. Thus, the relevant increase in the computational time due to the higher number of elements in the computational domain after the mesh refinement is not justified, as the difference in results compared to the initial case is minimal.

The time step independency of the results is evaluated considering the initial time step (ts) of 0.01 s, its double (ts=0.02 s) and its half (ts=0.005 s). As shown in Fig. 10b, the differences between the three simulations are lower than 2 %. Therefore, the same conclusions drawn for the grid independence analysis also apply to the time step sensitivity, confirming that the initial time step value is appropriate for conducting the simulations.

References

Ahluwalia, R.K., Roh, H.-S., Peng, J.-K., Papadias, D., Baird, A.R., Hecht, E.S., Ehrhart, B. D., Muna, A., Ronevich, J.A., Houchins, C., Killingsworth, N.J., Aceves, S.M., 2023. Liquid hydrogen storage system for heavy duty trucks: Configuration, performance, cost, and safety. Int. J. Hydrog. Energy 48, 13308–13323. https://doi.org/10.1016/j.ijhydene.2022.12.152.

Altair Engineering Inc, 2025. Material Data Center [WWW Document]. URL ⟨https://www.materialdatacenter.com/mb/⟩.

ANSYS Inc, 2018. Ansys Fluent User Guide, Release 18.2.

ASTM International, 2019. ASTM C740/C740M-13 - Standard Guide for Evacuated Reflective Insulation in Cryogenic Service, in: Cryogenic Service. West Conshohocken. https://doi.org/10.1520/C0740.

Aydemir, N.U., Magapu, V.K., Sousa, A.C.M., Venart, J.E.S., 1988. Thermal response analysis of LPG tanks exposed to fire. J. Hazard. Mater. 20, 239–262. https://doi.org/10.1016/0304-3894(88)87015-8.

Beynon, G.V., Cowley, L.T., Small, L.M., Williams, I., 1988. Fire engulement of LPG tanks: heatup, a predictive model. J. Hazard. Mater. 20, 227–238. https://doi.org/10.1016/0304-3894(88)87014-6.

Birk, A., Dusserre, G., Heymes, F., 2013. Analysis of a propane sphere BLEVE. Chem. Eng. Trans. 31, 481–486. https://doi.org/10.3303/CET1331081.

Bradley, I., Scarponi, G.E., Otremba, F., Birk, A.M., 2021. An overview of test standards and regulations relevant to the fire testing of pressure vessels. Process Saf. Environ. Prot. 145, 150–156. https://doi.org/10.1016/J.PSEP.2020.07.047.

Camplese, D., Chianese, C., Scarponi, G.E., Eberwein, R., Otremba, F., Cozzani, V., 2023. Analysis of High Temperature Degradation of Multi-Layer Insulation (MLI) Systems for Liquid Hydrogen Storage Tanks. Chem. Eng. Trans. 99, 415–420. https://doi.org/10.3303/CET2399070.

Camplese, D., Scarponi, G.E., Chianese, C., Hajhariri, A., Eberwein, R., Otremba, F., Cozzani, V., 2024. Modeling the performance of multilayer insulation in cryogenic tanks undergoing external fire scenarios. Process Saf. Environ. Prot. 186, 1169–1182. https://doi.org/10.1016/j.psep.2024.04.061.

Camplese, D., Scarponi, G.E., Eberwein, R., Hajhariri, A., Otremba, F., Cozzani, V., 2025. Comparative performance assessment of multilayer insulation (MLI) systems for liquid hydrogen vessels in fire scenarios. Int. J. Hydrog. Energy 135, 537–552. https://doi.org/10.1016/j.ijhydene.2025.04.534.

Chen, H.-J., Lin, M.-H., 1999. Modeling a Boiling-Liquid, Expanding-Vapor Explosion Phenomenon with Application to Relief Device Design for Liquefied Ammonia Storage. Ind. Eng. Chem. Res. 38, 479–487. https://doi.org/10.1021/ie980216y.

Cirrone, D., Makarov, D., Molkov, V., 2023. Rethinking “BLEVE explosion” after liquid hydrogen storage tank rupture in a fire. Int. J. Hydrog. Energy 48, 8716–8730. https://doi.org/10.1016/j.ijhydene.2022.09.114.

Cocchi, G., 2022. The Bologna LPG BLEVE, in: International Colloquium on the Dynamics of Explosions and Reactive Systems (ICDERS). Naples, Italy, pp. 1–6.

D’Aulisa, A., Tugnoli, A., Cozzani, V., Landucci, G., Birk, A.M., 2014b. CFD modeling of LPG vessels under fire exposure conditions. AIChE J. 60, 4292–4305. https://doi.org/10.1002/aic.14599.

D’Aulisa, A., Simone, D., Landucci, G., Tugnoli, A., Cozzani, V., Birk, A.M., 2014a. Numerical simulation of tanks containing pressurized gas exposed to accidental fires: evaluation of the transient heat up. Chem. Eng. Trans. 36, 241–246. https://doi.org/10.3303/CET1436041.

Eberwein, R., Hajhariri, A., Camplese, D., Scarponi, G.E., Cozzani, V., Otremba, R., 2023. Insulation materials used in tanks for the storage of cryogenic fluids in fire scenarios, in: Proceedings of the ASME 2023 Pressure Vessel and Piping Conference (PVP2023). https://doi.org/10.1115/PVP2023-105201.

Eberwein, R., Hajhariri, A., Camplese, D., Scarponi, G.E., Cozzani, V., Otremba, F., 2024a. Experimental investigation on the behavior of thermal super insulation materials for cryogenic storage tanks in fire incidents. Process Saf. Environ. Prot. 187, 240–248. https://doi.org/10.1016/j.psep.2024.04.131.

Eberwein, R., Hajhariri, A., Camplese, D., Scarponi, G.E., Cozzani, V., Otremba, F., 2024b. Experimental Research Of A Tank For A Cryogenic Fluid With A Wall Rupture In A Fire Scenario, in: 15th International Symposium on Hazards, Prevention, and Mitigation of Industrial Explosions. Naples. https://doi.org/https://doi.org/10.5281/zenodo.12621001.

Feynman, R., 1986. Report of the presidential commission on the space shuttle Challenger accident. Append. F 7.

Gong, Y.W., Lin, W.S., Gu, A.Z., Lu, X.S., 2004. A simplified model to predict the thermal response of PLG and its influence on BLEVE. J. Hazard. Mater. 108, 21–26. https://doi.org/10.1016/j.jhazmat.2004.01.012.

Graves, K.W., 1973a. Development of a Computer Model for Modeling the Heat Effects on a Tank Car. US Department of Transportation, Federal Railroad Administration, Washington DC.

Graves, K.W., 1973b. Development of a computer program for modeling the heat effects on a railroad tank car. No. FRA-OR&D 75-33 Final Rpt.

Hadjisophocleous, G.V., Sousa, A.C.M., Venart, J.E.S., 1990b. Mathematical modelling of LPG tanks subjected to full and partial fire engulfment. Int. J. Numer. Methods Eng. 30 (4), 629–646. https://doi.org/10.1002/nme.1620300406.

Hadjisophocleous, G.V., Sousa, A.C.M., Venart, J.E.S., 1990a. A study of the effect of the tank diameter on the thermal stratification in LPG tanks subjected to fire engulfment. J. Hazard. Mater. 25, 19–31. https://doi.org/10.1016/0304-3894(90)85067-D.

Hajhariri, A., Eberwein, R., Perrone, L.P., Cozzani, V., Otremba, F., Seidlitz, H., 2024. Study the impact of spacer at thermal degradation process of MLI-based insulation in fire condition. J. Loss Prev. Process Ind. 92, 105461. https://doi.org/10.1016/j.jlp.2024.105461.

Hajhariri, A., Eberwein, R., Camplese, D., Scarponi, G.E., Cozzani, V., Otremba, F., Seidlitz, H., 2025. Non-combustible MLI based insulation behavior under fire condition - Experimental and numerical investigation. Process Saf. Environ. Prot. 193, 403–420. https://doi.org/10.1016/j.psep.2024.11.037.

Hirt, C., Nichols, B., 1981. Volume of fluid (VOF) method for the dynamics of free boundaries. J. Comput. Phys. 39, 201–225. https://doi.org/10.1016/0021-9991(81)90145-5.

Howell, J., Siegel, R., Mengüç, M.P., 2010. Thermal Radiation Heat Transfer, Fifth. ed. https://doi.org/10.1201/9781439894552.
Hulsbosch-Dam, C., Atli-Veltin, B., Kamperveen, J., Velthuis, H., Reinders, J., Spruijt, M., Vredeveldt, L., 2017. Thermodynamic aspects of an LNG tank in fire and experimental validation, in: EPJ Web of Conferences. EDP Sciences. https://doi.org/10.1051/epjconf/201714302039.
Hunt, D.L.M., Ramskill, P.K., 1985. The behaviours of tanks engulfed in fire - The development of a computer program. IChemE Symp. Ser. 93, 71–86.
HydrogenTools Liquid, 2017. Liquid hydrogen tank boiling liquid expanding vapor explosion (BLEVE) due to water-plugged vent stack [WWW Document]. URL ⟨https://h2tools.org/lessons/liquid-hydrogen-tank-boiling-liquid-expanding-vapor-explosion-bleve-due-water-plugged-vent⟩ (accessed 12.12.24).
Iannaccone, T., Scarponi, G.E., Landucci, G., Cozzani, V., 2021. Numerical simulation of LNG tanks exposed to fire. Process Saf. Environ. Prot. 149, 735–749. https://doi.org/10.1016/j.psep.2021.03.027.
Jiang, W., Sun, P., Li, P., Zuo, Z., Huang, Y., 2021. Transient thermal behavior of multi-layer insulation coupled with vapor cooled shield used for liquid hydrogen storage tank. Energy 231, 120859. https://doi.org/10.1016/j.energy.2021.120859.
Kang, D.-H., An, J.-H., Lee, C.-J., 2024. Numerical modeling and optimization of thermal insulation for liquid hydrogen storage tanks. Energy 291, 130143. https://doi.org/10.1016/j.energy.2023.130143.
Kangwanpongpan, T., Makarov, D.V., Cirrone, D., Molkov, V., 2023. Numerical simulation of liquid hydrogen evaporation in the pressurized tank during venting. International Conference on Hydrogen Safety, Québec, Canada, pp. 1–13.
Klell, M., 2010. Storage of Hydrogen in the Pure Form. In: Hirscher, M. (Ed.), Handbook of Hydrogen Storage. John Wiley & Sons, Ltd, Weinheim, Germany, pp. 1–37. https://doi.org/10.1002/9783527629800.
Launder, B.E., Spalding, D.B., 1983. THE NUMERICAL COMPUTATION OF TURBULENT FLOWS, in: Patankar, S. V, Pollard, A., Singhal, A.K., Vanka, S.P. (Eds.), Numerical Prediction of Flow, Heat Transfer, Turbulence and Combustion. Pergamon, pp. 96–116. https://doi.org/https://doi.org/10.1016/B978-0-08-030937-8.50016-7.
Lee, W.H., 1980. A Pressure Iteration Scheme for Two-Phase Flow Modeling. Multiph. Transp. Fundam. React. Saf. Appl. 1, 407–431. https://doi.org/10.1142/9789814460286_0004.
Liu, C.-Y., Lees, L., 1961. Kinetic Theory Description of Plane, Compressible Couette Flow. Rarefied Gas. Dyn. 391–428.
Liu, Z., Li, Y., Zhou, G., 2018. Study on thermal stratification in liquid hydrogen tank under different gravity levels. Int. J. Hydrog. Energy 43, 9369–9378. https://doi.org/10.1016/j.ijhydene.2018.04.001.
Mcintosh, G.E., 1994. Layer by Layer MLI Calculation Using a Separated Mode Equation. In: Kittel, P. (Ed.), Advances in Cryogenic Engineering. Springer, Boston. https://doi.org/10.1007/978-1-4615-2522-6_206.
Mires, R.W., 1985. Analysis of liquid hydrogen explosion. Phys. Teach. 23, 533–535. https://doi.org/10.1119/1.2341906.
Moodie, K., Cowley, L.T., Denny, R.B., Small, L.M., Williams, I., 1988. Fire engulfment tests on a 5 tonne LPG tank. J. Hazard. Mater. 20, 55–71. https://doi.org/10.1016/0304-3894(88)87006-7.
National Institute of Standards and Technology, 2021. NIST Chemistry WebBook, SRD 69: Thermophysical Properties of Fluid Systems [WWW Document]. URL ⟨https://webbook.nist.gov/chemistry/fluid/⟩.
Nubli, H., Wen, J.X., 2025. Pressure build-up in a liquid hydrogen storage tank when subject to fire attack – a numerical study with validation. Int. J. Hydrog. Energy 193, 152373. https://doi.org/10.1016/j.ijhydene.2025.152373.
Ødegård, A., Sommerseth, C., Odsæter, L.H., Skarsvåg, H.L., Nekså, P., Meraner, C., Stølen, R., Li, T., Muthusamy Deiveegan, Van Wingerden, K., Siccama, D., Gawas, Y., Ustolin, F., George, C., 2022. D5.4: SH2IFT final project report.
Pehr, K., 1996b. Aspects of safety and acceptance of LH2 tank systems in passenger cars. Int. J. Hydrog. Energy 21, 387–395.
Pehr, K., 1996a. Experimental examinations on the worst-case behaviour of LH2/LNG tanks for passenger cars, in: Proc. 11th World Hydrogen Energy Conference. Stuttgart, Germany.
Planas, E., Pastor, E., Casal, J., Bonilla, J.M., 2015. Analysis of the boiling liquid expanding vapor explosion (BLEVE) of a liquefied natural gas road tanker: The Zarzalico accident. J. Loss Prev. Process Ind. 34, 127–138. https://doi.org/10.1016/j.jlp.2015.01.026.
Ramskill, P.K.K., 1988. A description of the “engulf” computer codes - Codes to model the thermal response of an LPG tank either fully or partially engulfed by fire. J. Hazard. Mater. 20, 177–196. https://doi.org/10.1016/0304-3894(88)87012-2.
Scarponi, G.E., Landucci, G., Birk, A.M., Cozzani, V., 2018. LPG vessels exposed to fire: Scale effects on pressure build-up. J. Loss Prev. Process Ind. 56, 342–358. https://doi.org/10.1016/j.jlp.2018.09.015.
Scarponi, G.E., Landucci, G., Birk, A.M., Cozzani, V., 2019. An innovative three-dimensional approach for the simulation of pressure vessels exposed to fire. J. Loss Prev. Process Ind. 61, 160–173.
Scarponi, G.E., Landucci, G., Birk, A.M., Cozzani, V., 2021. Three dimensional CFD simulation of LPG tanks exposed to partially engulfing pool fires. Process Saf. Environ. Prot. 150, 385–399. https://doi.org/10.1016/j.psep.2021.04.026.
Scarponi, G.E., Cozzani, V., Antonioni, G., Doghieri, F., 2024. Modeling the behavior of LPG tanks exposed to partially engulfing pool fires. Process Saf. Environ. Prot. 182, 1072–1085. https://doi.org/10.1016/j.psep.2023.12.048.
Shebeko, Y., Bolodian, I.A., Filippov, V.N., Navzenya, V.Y., Kostyuhin, A.K., Tokarev, P. M., Zamishevski, E.D., 2000. A study of the behaviour of a protected vessel containing LPG during pool fire engulfment. J. Hazard. Mater. 77, 43–56. https://doi.org/10.1016/S0304-3894(00)00247-8.
Sherman, F.S., 1963. A Survey of Experimental Results and Methods for the Transition Regime of Rarified Gas Dynamics. Rarefied Gas. Dyn. 2, 228.
Sumathipala, U.K., Hadjisophocleous, G.V., Aydemir, N.U., Yu, C.-M., Sousa, A.C.M., Steward, F.R., Venart, J.E.S., 1992. Fire engulfment of pressure-liquefied gas tanks: Experiments and modeling. Fire Hazard Fire Risk Assess. 1150, 100–111.
Tzimas, E., Filou, C., Peteves, S., Veyret, J.-B., 2003. Hydrogen storage: state-of-the-art and future perspective. EU Comm. JRC Petten, EUR 20995EN 1511–1519.
Ustolin, F., Iannaccone, T., Cozzani, V., Jafarzadeh, S., Paltrinieri, N., 2021. Time to Failure Estimation of Cryogenic Liquefied Tanks Exposed to a Fire, in: 31st European Safety and Reliability Conference. Angers, France, pp. 935–942. https://doi.org/10.3850/978-981-18-2016-8_182-cd.
Ustolin, F., Scarponi, G.E., Iannaccone, T., Cozzani, V., Paltrinieri, N., 2022. Cryogenic Hydrogen Storage Tanks Exposed to Fires: a CFD Study. Chem. Eng. Trans. 90, 535–540. https://doi.org/10.3303/CET2290090.
Wang, B., Huang, Y.H., Li, P., Sun, P.J., Chen, Z.C., Wu, J.Y., 2016. Optimization of variable density multilayer insulation for cryogenic application and experimental validation. Cryog. (Guildf.) 80, 154–163. https://doi.org/10.1016/j.cryogenics.2016.10.006.
Xie, G.F., Li, X.D., Wang, R.S., 2010. Study on the heat transfer of high-vacuum-multilayer-insulation tank after sudden, catastrophic loss of insulating vacuum. Cryog. (Guildf.) 50, 682–687. https://doi.org/10.1016/j.cryogenics.2010.06.020.
Yu, C.M., Aydemir, N.U., Venart, J.E.S., 1992. Transient free convection and thermal stratification in uniformly-heated partially-filled horizontal cylindrical and spherical vessels. J. Therm. Sci. 1, 114–122. https://doi.org/10.1007/BF02650847.